

▶▶
UHASSELT



Maastricht University

KNOWLEDGE IN ACTION

Faculty of Medicine and Life Sciences **School for Life Sciences**

Master of Biomedical Sciences

Master's thesis

The role of lysosomal cathepsins D and B in Charcot-Marie-Tooth disease type 1A

Nathalie Dirkx

Thesis presented in fulfillment of the requirements for the degree of Master of Biomedical Sciences, specialization
Molecular Mechanisms in Health and Disease

SUPERVISOR :

Prof. dr. Esther WOLFS

MENTOR :

Mevrouw Karen LIBBERECHT

Transnational University Limburg is a unique collaboration of two universities in two countries: the University of Hasselt and Maastricht University.



UHASSELT

KNOWLEDGE IN ACTION

www.uhasselt.be
Universiteit Hasselt
Campus Hasselt:
Martelarenlaan 42 | 3500 Hasselt
Campus Diepenbeek:
Agoralaan Gebouw D | 3590 Diepenbeek

2021
2022



Maastricht University

Faculty of Medicine and Life Sciences

School for Life Sciences

Master of Biomedical Sciences

Master's thesis

The role of lysosomal cathepsins D and B in Charcot-Marie-Tooth disease type 1A

Nathalie Dirkx

Thesis presented in fulfillment of the requirements for the degree of Master of Biomedical Sciences, specialization
Molecular Mechanisms in Health and Disease

SUPERVISOR :

Prof. dr. Esther WOLFS

MENTOR :

Mevrouw Karen LIBBERECHT

The role of lysosomal cathepsins D and B in Charcot-Marie-Tooth disease type 1A *

Dirkx N.¹, Libberecht K.^{2,3}, Vangansewinkel T.^{2,3}, Jeurissen H.², van den Bosch J.², Lambrichts I.², Van Den Bosch L.^{3,4}, and Wolfs E.²

¹UHasselt, Faculty of Medicine and Life Sciences, Agoralaan, 3590 Diepenbeek, Belgium.

²UHasselt, FIERCE lab, Cardio-and Organ Systems, BIOMED, Agoralaan, 3590 Diepenbeek, Belgium.

³VIB, Center for Brain & Disease Research, Laboratory of Neurobiology, 3000 Leuven, Belgium.

⁴KU Leuven, Experimental Neurology, Leuven Brain Institute, 3000 Leuven, Belgium.

*Running title: *The role of cathepsins D and B in CMT1A*

To whom correspondence should be addressed: Wolfs Esther, Tel: +32 11 26 92 96; Email: esther.wolfs@uhasselt.be

Keywords: Charcot-Marie-Tooth disease type 1A – PMP22 - Schwann cells - Proteostasis – Lysosomes - Cathepsins – Patient-in-a-dish model

ABSTRACT

Charcot-Marie-Tooth disease type 1A (CMT1A) is the most prevalent demyelinating peripheral neuropathy worldwide. CMT1A is caused by a duplication of the *peripheral myelin protein 22 (PMP22)* gene, resulting in Schwann cell dysfunction. High levels of misfolded PMP22 aggregates have been demonstrated to overload Schwann cell proteasomes, impairing protein clearance in CMT1A. Hence, we aimed to assess the role of PMP22 misfolding at the lysosomal level. Our results provide strong evidence for a compensatory lysosomal upregulation upon proteasomal impairment in CMT1A. Lysosomal and autophagic proteins were increased in C3 mouse nerves throughout their lifespan, in pure primary C3 mouse Schwann cell populations, and in a human patient-in-a-dish model for CMT1A. Furthermore, we report substantial increases in lysosomal cathepsins D (CTD) and B (CTB) in the nerve tissue of C3 mice at the ages of two, four, and eight weeks and at one year of age. We confirmed these results in a pure primary Schwann cell population and in a human-patient-in-a-dish model using CMT1A patient-derived induced Pluripotent Stem Cells (iPSC) differentiated into Schwann cell precursors (iPSC-SCP).

Our results demonstrate that lysosomal enzymes play a crucial role in CMT1A development and progression. Hence, we propose selective CTD and CTB inhibitors as promising therapies for CMT1A patients.

INTRODUCTION

Charcot-Marie-Tooth disease (CMT), or hereditary motor and sensory neuropathy (HMSN), is the most common inherited peripheral neuropathy, with an overall prevalence of one in 2,500 (1-3). CMT affects both sensory and motor nerves, causing muscle weakness and atrophy, loss of stretch reflexes, decreased sensitivity to touch, and foot deformities such as *pes cavus*, foot drop, and hammertoes. These symptoms typically begin in the first two decades of life and slowly progress in proximal and ascending directions (1, 2). To date, CMT is treated symptomatically using medical support devices, rehabilitation therapy, corrective surgery for skeletal deformities, and pain medication, highlighting the urgent need to thoroughly understand the pathology in order to develop disease-modifying treatments (1, 3).

CMT comprises a heterogeneous group of disorders, categorized into two main types based on the dominant clinical phenotype. The primary demyelinating CMT type 1 (CMT1) is the most prevalent disease form and is characterized by nerve conduction velocities (NCVs) below 38 m/s, whereas patients with the primary axonal CMT type 2 (CMT2) display near-normal or mildly reduced NCVs between 38 and 45 m/s (1, 2). In addition, intermediate CMT types are discerned, including the rare CMT3 and CMT4 forms, which cause more severe clinical manifestations with both myelin and axonal abnormalities, and CMTX, which is distinguished based on its X-linked inheritance pattern (2, 4). Moreover, all disease

types are further subdivided according to over 45 known causative genes (2).

CMT1A is the most prevalent of all CMT cases and is caused by a 1.5 Mb tandem duplication of the short arm of chromosome 17 (2, 5, 6). This region contains the *peripheral myelin protein 22* (*PMP22*) gene, which has been described to be responsible for the CMT1A phenotype (5, 7). *PMP22* is predominantly expressed by Schwann cells, the myelinating cells of the peripheral nervous system (2). Although the exact functions of *PMP22* in Schwann cells remain largely unknown (7, 8), this aggregation-prone 22 kDa membrane glycoprotein is believed to play a crucial role in myelin stability (5, 9, 10).

Under physiological conditions, only 20% of the newly synthesized *PMP22* fully matures and traffics to the cellular membrane. Meanwhile, 80% of *PMP22* misfolds and is, therefore, rapidly degraded to maintain proteostasis (6, 7, 11). The ubiquitin-proteasome system (UPS) is the first line of defense against misfolded *PMP22*, in which the protein is targeted by polyubiquitin chains for degradation by the multiunit proteasome complex (8, 10). Since the UPS capacity is limited (8), it is not surprising that high *PMP22* levels overload and impair the proteolytic system, hence reducing protein turnover (7, 8, 10, 12). However, upon UPS overload, activation of the lysosomal-autophagic pathway can compensate for the protein burden that arises (8).

Lysosomes are acidic organelles with a phospholipid bilayer membrane ensuring the confinement of hydrolytic enzymes, which degrade endo- and exogenous cargo, including proteins, lipids, and pathogens (13, 14). Lysosomes degrade intracellular components during (macro)autophagy, in which double-membrane bound autophagosomes engulf misfolded proteins, aggregates, or organelles and subsequently fuse with lysosomes to degrade the cargo (10, 15). In CMT1A, upregulated lysosomal and autophagic markers have been demonstrated to co-localize with misfolded *PMP22* aggregates (10, 12). Hence, Schwann cells presumably make use of this autophagy-dependent lysosomal degradation to clear misfolded *PMP22* aggregates. Nevertheless, the persisting presence of *PMP22* aggregates in CMT1A patients and animal models indicates that the activation of the lysosomal-autophagy pathway is insufficient to clear all accumulated *PMP22* (15). Interestingly,

the lysosomal accumulation of aggregated proteins has previously been recognized as a risk factor for lysosomal exocytosis and lysosomal membrane permeabilization (LMP), which result in the leakage of lysosomal enzymes into the extracellular matrix (ECM) and the cytosol, respectively (14, 16-19). Upon reaching the cytosol, lysosomal enzymes can cause severe damage and, in some cases, even induce cell death (13, 19, 20).

Cathepsins D (CTD) and B (CTB) are ubiquitously and abundantly present in the lysosomal compartment, where they exert their primary homeostatic function by degrading intracellular proteins during autophagy (13, 21). Interestingly, recent research has demonstrated CTD and CTB to remain stable in neutral and slightly alkaline pH ranges, such as in the cytosol and ECM (16, 22-24). While extracellular CTD activity appears to be attributable to pro-CTD forms (24), CTB acquires high extracellular stability via attachment to large ECM proteins (23, 25). Moreover, CTD and CTB are capable of ECM remodeling by degrading extracellular proteins, including collagen, laminin, and fibronectin (26-28). Hence, lysosomal exocytosis can lead to the loss of Schwann cell-ECM interactions, which are vital to maintaining the myelinating Schwann cell phenotype (29, 30). In support of this hypothesis, ECM remodeling has been reported in peripheral neuropathies, with collagen, laminin, and fibronectin changes being demonstrated in CMT1 patient nerve biopsies and CMT1A animal models (31-34).

In the past, CMT1A research has been hindered by challenges in disease modeling. Therefore, many findings were based on the naturally occurring Trembler J mice, representing a CMT1A-like phenotype due to a *PMP22* mutation (33). More recently, rodent models harboring *PMP22* duplications have been constructed. The transgenic C22 mouse model was the first *PMP22*-overexpressing animal, generated using human *PMP22* yeast artificial chromosomal (YAC) constructs (35). These C22 mice express seven copies of the human *PMP22* gene, resulting in a clinical phenotype that is generally more severe than in human CMT1A patients. Hence, transgenic animals with low copy numbers, including the C3 mice, better mimic the human disease and constitute a more appropriate model for CMT1A disease studies (36). The YAC transgenic C3 mouse

model expresses three to four *PMP22* copies and displays a mild phenotype that correlates well with the human pathology (36).

Nevertheless, although rodent models have led to important insights into CMT1A, they do not entirely recapitulate the human disease, as illustrated by previous failures in clinical translation. For instance, ascorbic acid was proven to improve myelination and disease phenotype in animal models but did not show any benefits in human trials (37). Hence, human-specific CMT1A models are essential to further elucidate the underlying pathology and bridge the gap between preclinical and clinical research. However, the isolation of human Schwann cells is unethical since it requires invasive nerve resection surgery, which can cause damage to healthy tissue, and results in a low proliferative yield (38). Induced Pluripotent Stem Cells (iPSC) can overcome these limitations and have been successfully used to generate premature Schwann cell precursors (iPSC-SCP) (33). Although the *PMP22* overexpression has been induced in healthy donor iPSC to mimic CMT1A (33), we have successfully created a human patient-in-a-dish iPSC-SCP model that recapitulates the entire CMT1A pathology in a high yield of immature Schwann cells. This *in vitro* model has the additional advantage of revealing the direct effects of the CMT1A genotype, particularly on the Schwann cell phenotype and myelination (5, 33). Combined with the C3 mouse model, this human patient-in-a-dish-model thus constitutes a highly translatable research platform to validate our findings, supporting information transfer to clinical trials.

We propose a link between *PMP22* aggregation, lysosomal permeability, and peripheral nerve ECM remodeling in the aberrant differentiation of CMT1A Schwann cells. As a starting point, this article aims to investigate the role of *PMP22* duplication and misfolding at the lysosomal level over the lifespan of the C3 animal model and in a human patient-in-a-dish model for CMT1A. Our results demonstrate the *PMP22* duplication to induce lysosomal upregulation and cathepsin elevations in C3 mice and human stem cell-derived Schwann cell precursors. Ultimately, this might result in lysosomal exocytosis, LMP, and the release of lysosomal cathepsins into the cell and the ECM.

EXPERIMENTAL PROCEDURES

Animals – Heterozygous C3 and homogeneous wild type (WT) C57BL/6J mice were kindly provided by Prof. Dr. Frank Baas (LUCM, The Netherlands). Mice were bred and housed according to the guidelines of Hasselt University with four to five animals per cage in a temperature-controlled room ($\pm 20^{\circ}\text{C}$) and with *ad libitum* access to food and water. All experimental animal procedures were approved by the Ethical Committee for Animal Experimentation (ECAE) of Hasselt University. Genotyping was performed on ear biopsies using polymerase chain reaction (PCR) to identify human *PMP22* with the following primer pair: forward (F) 5' TGG TGA TGA TGA GAA ACA GT 3' and reverse (R) 5' TGA TTC TCT CTA GCA ATG GA 3'.

Nerve isolation and Schwann cell isolation – C3 and WT mice were sacrificed by cervical dislocation at the ages of two, four, and eight weeks and one year old. The sciatic and brachial plexus nerves were isolated as described by Andersen et al. (39). Briefly, Schwann cells were isolated from freshly harvested peripheral nerves through the removal of the epineurium, mechanical teasing and dissociation, and enzymatic dissociation with collagenase I and dispase II. Following overnight incubation at 37°C and 9% CO_2 , cells were droplet plated on poly-L-lysine (PLL) coated 100 mm cell culture dishes (Sigma-Aldrich, St. Louis, MO, USA). Primary Schwann cells were proliferated in Dulbecco's Modified Eagle Medium (DMEM) (Thermo Fisher Scientific, Waltham, MA, USA, Gibco), supplemented with 10% fetal bovine serum (FBS), 2 μM forskolin, 10 μM neuregulin (NRG), 5 ng/ml platelet-derived growth factor AA (PDGF-AA), and 1% penicillin/streptomycin (P/S). The medium was changed three times per week. Next, Schwann cells were sorted by fluorescence-activated cell sorting (FACS) following incubation with FITC-conjugated anti-mouse CD90.2 (Thy-1.2) antibody (BioLegend, San Diego, CA, USA; Ref. 140303) for 20 min at room temperature (RT).

Cell culture – Primary C3 and WT Schwann cells were cultured in high proliferation DMEM supplemented with 10% FBS, 2 μM forskolin, 10 μM NRG, 5 ng/ml PDGF-AA, and 1% P/S, as described by Andersen et al. (39), at 37°C in a 9% CO_2 incubator. Three medium changes were performed per week.

Dermal fibroblasts were harvested from CMT1A patients with informed consent and reprogrammed into iPSC in the lab of Prof. Dr. Ludo Van Den Bosch (VIB-KU Leuven, Belgium). Undifferentiated patient-derived iPSC and control iPSC (Sigma-Aldrich) were cultured on Matrigel hESC-qualified Matrix (Corning, NY, USA; Ref. 354277) coated 6-well-plates in E8 Flex medium (Thermo Fisher Scientific, Gibco) with E8 supplement at 37°C and 5% CO₂. Medium changes were performed three times per week.

iPSC-SCP were obtained by differentiation of the patient-derived iPSC and were provided by Prof. Dr. Van Den Bosch. Isogenic control lines were generated through TALEN-mediated repair of the *PMP22* duplication. iPSC-SCP were cultured on Matrigel Matrix (Corning, Ref. 356231) precoated flasks in a 5% CO₂ incubator at 37°C. iPSC-SCP medium consisted of DMEM F-12 (Thermo Fisher Scientific) and neurobasal medium (Thermo Fisher Scientific), supplemented with 2 mM Glutamax, 0.01% N2, 0.02% B27, 20 µM SB 431542, 3 µM Chir 99021, 50 ng/ml NRG, 0.005% bovine serum albumin (BSA), 0.11 mM β-mercaptoethanol (BME), and 0.01% P/S, and was changed three times per week.

Quantitative PCR (qPCR) – Cells (3x10⁴/well) were seeded on 24-well plates until confluent, while sciatic and brachial plexus nerves were frozen in liquid nitrogen (LN₂) and stored at -80°C until further use. Total mRNA was extracted from cells and nerves using QIAzol Lysis reagent (Qiagen, Hilden, Germany). After assessing the RNA concentration and quality by NanoDrop (Thermo Fisher Scientific), 3 ng/µL cDNA samples were synthesized using Qscript (Quantabio, Beverly, MA, USA) and a T-100 Thermal Cycler (Bio-Rad, Hercules, CA, USA). Finally, qPCR SYBR Green (Thermo Fisher Scientific, Applied Biosystems) master mixes, including primer pairs (Supplementary Table 1), were added to the samples. Primer efficiencies were verified for all primer pairs. Ct values, detected by Quant Studio (Thermo Fisher Scientific, Applied Biosystems), were used to determine the fold change (FC) normalized for validated housekeeping genes.

Western blot (WB) – Nerves were frozen in LN₂ and stored at -80°C. For protein isolation, nerves were incubated with RIPA buffer supplemented with a protease inhibitor cocktail (Roche Diagnostics, Basel, Switzerland) for 20 min

at RT. Next, tissue lysates were centrifuged at 13,000 g for 10 min at 4°C. Protein levels were quantified using the Pierce BCA protein assay kit (Thermo Fisher Scientific), according to the manufacturer's instructions, and with BSA as a protein standard. The absorbance at 570 nm was read by an iMark Microplate Reader (Bio-Rad). Subsequently, Precision Plus Protein Dual Color Standard ladder (Bio-Rad) and 5 µg/mL samples were loaded in 12% gels and separated via sodium dodecyl sulfate-polyacrylamide gel electrophoresis (SDS-PAGE) at 200 V for 45 min. Following protein transfer to a polyvinylidene difluoride (PVDF) membrane at 350 mA for 2h, blocking was performed in 5% Marvel PBS for 1h at RT. Next, the PVDF membrane was incubated overnight at 4°C with primary antibody (Supplementary Table 2). The following day, blots were washed in 0.05% Tween-20 PBS and incubated with 1/2,000 HRP-conjugated polyclonal rabbit anti-rat (P0450), goat anti-rabbit (P0448), or goat anti-mouse (P0447) secondary antibodies purchased from Dako, Santa Clara, CA, USA. Afterward, antibodies were stripped from the membrane, and the steps were repeated for the β-actin reference protein (Supplementary Table 2). Using the chemiluminescent Amersham Imager 680 (Thermo Fisher Scientific), lysosomal proteins were detected with the ECLPlus SuperSignal™ West Atto Ultimate Sensitivity Substrate (Thermo Fisher Scientific, Ref. A38555), while the Pierce ECL Plus Western Blotting Substrate (Thermo Fisher Scientific, Ref. 32132) was used for β-actin detection. Finally, protein bands were analyzed by Imagequant TL 8.2 software (Cytiva, Marlborough, MA, USA) and normalized for β-actin.

Immunocytochemistry (ICC) – Cells (10x10⁴/well) were seeded on glass coverslips in Matrigel-coated 24-well plates in culture medium. After reaching 80-90% confluence, the cells were fixed in 4% paraformaldehyde (PFA) and washed with PBS. Cells were permeabilized for 15 min with 0.05% Tween-20 PBS, washed, and blocked with 10% Protein block serum-free (Dako) for 1h at RT. After overnight incubation at 4°C with primary antibody (Supplementary Table 2), cells were incubated with 1/300 secondary Alexa Fluor (AF) 555 goat anti-rat (A21434), AF 647 goat anti-rabbit (A21430), and AF 488 goat anti-mouse (A28175) or AF 488 donkey anti-mouse (A21202) and AF 555 donkey anti-rabbit (A31572) antibodies

(Thermo Fisher Scientific) for 1h at RT. Negative controls without primary antibody were included, and nuclei were counterstained with DAPI (Thermo Fisher Scientific, Ref. 62248) for 30 min at RT. Following a final washing step, coverslips were mounted using Immunomount (Thermo Fisher Scientific). Fluorescent images were acquired with a Leica DM4000 B LED microscope (Leica Microsystems) and analyzed with Image J (Fiji) (Version 2.1.0/1.53c) following thresholding to obtain the integrated density (area x mean), normalized for cell number.

Immunohistochemistry (IHC) – Sciatic nerves were fixed overnight with 4% PFA, washed with PBS, and cryopreserved. Coronal 10 µm sections were obtained using a Leica CM3050 S cryostat (Leica Biosystems, Wetzlar, Germany) and stored at -80°C until further use. Mild antigen retrieval was performed by treatment with microwaved citrate buffer for 7 min. Sections were washed with PBS, blocked for 1h with 100% Protein block serum-free, and treated with primary antibody (Supplementary Table 2), while negative controls were treated with 10% Protein block instead. After overnight incubation at 4°C, nerves were treated for 2h with 1/300 AF 488 goat anti-rat (A11006), AF 555 goat anti-rat (A21434), AF 647 goat anti-rat antibodies (A21247), AF 555 goat anti-rabbit (A21430), and AF 647 goat anti-rabbit (A21245) antibodies (Thermo Fisher Scientific) and washed. DAPI was added for 30 min at RT, and slices were washed before mounting with Immunomount. Images were acquired with a Leica DM4000 B LED microscope, thresholded, and analyzed by ImageJ to calculate the %area (area/total area) and integrated density (%area x mean) of the sciatic nerves. Means were calculated from three representative nerve sections per mouse.

Statistical analysis – Statistics were performed by GraphPad Prism version 9.3.1 (350) (GraphPad Software, San Diego, CA, USA). Statistical outliers were removed for analysis. Following the Shapiro-Wilk test for normality, data were accordingly analyzed by the Multiple Unpaired t-tests, or the Mann-Whitney Multiple tests, with Bonferroni-Dunn correction for multiple comparisons. For non-multiple comparisons, the Unpaired t-test was used. Equality of variances was tested and corrected for by Welch's correction upon significant differences. P-values of ≤0.05 were considered significant.

RESULTS

Characterization of lysosome-associated mRNA changes over the lifespan of C3 nerve tissue - To obtain an in-depth analysis of lysosomal changes throughout the lifespan of C3 mice, we determined the relative mRNA changes in the nerve tissue of C3 mice compared to WT mice at the ages of two, four, and eight weeks and one year (**Fig 1**). For this purpose, mRNA was extracted from mouse sciatic and brachial plexus nerves to assess the relative expression of *lysosomal-associated membrane protein 1 (LAMP-1)*, *CTD*, *CTB*, *cathepsin S (CTS)*, *P62*, and *PMP22*.

At all observed ages, human *PMP22* mRNA expression significantly confirmed the animals' genotyping (**Fig 1a-d**). Since human *PMP22* could not be detected in WT nerves, FC could not be calculated and, thus, Ct values were plotted on the graphs (two weeks: Ct=23.061 ± 0.364, $p=0.0130$; four weeks: Ct=25.956 ± 0.922, $p<0.001$; eight weeks: Ct=31.199 ± 1.002, $p<0.001$; one year: Ct=31.467 ± 1.213, $p<0.001$).

In two-week-old C3 mice, the relative mRNA expression levels of *LAMP-1* and *CTD* increased to similar degrees, respectively by 1.203-fold (SEM ± 0.218, $p>0.999$) and 1.222-fold (SEM ± 0.178, $p>0.999$) in comparison to WT animals (**Fig 1a**). Furthermore, *CTB* expression was slightly elevated (FC=1.025 ± 0.091, $p>0.999$) compared to WT nerves, and relative *CTS* mRNA levels were highest with a 1.687-fold overexpression (SEM ± 0.299, $p=0.114$). In contrast, relative *P62* mRNA levels were slightly downregulated (FC=0.935 ± 0.139, $p>0.999$) in C3 animals at two weeks.

At four weeks of age, *LAMP-1* mRNA levels were slightly lower (FC=0.921 ± 0.138, $p>0.999$) in C3 *versus* WT mice, while all other lysosome-related genes were increased (**Fig 1b**). At this age, the relative mRNA expression increased by 1.842-fold (SEM ± 0.199, $p=0.128$) for *CTD*, 1.542-fold (SEM ± 0.143, $p=0.088$) for *CTB*, and 2.009-fold (SEM ± 0.285, $p=0.151$) for *CTS* in C3 nerve tissue. Simultaneously, *P62* became upregulated by 1.129-fold (SEM ± 0.169, $p>0.999$) compared to WT littermates.

All lysosome-associated relative mRNA expression levels reached peak overexpression in eight-week-old C3 mouse nerves (**Fig 1c**), except for *CTS*, which peaked at the age of four weeks (**Fig 1b**). Relative mRNA expression increased by

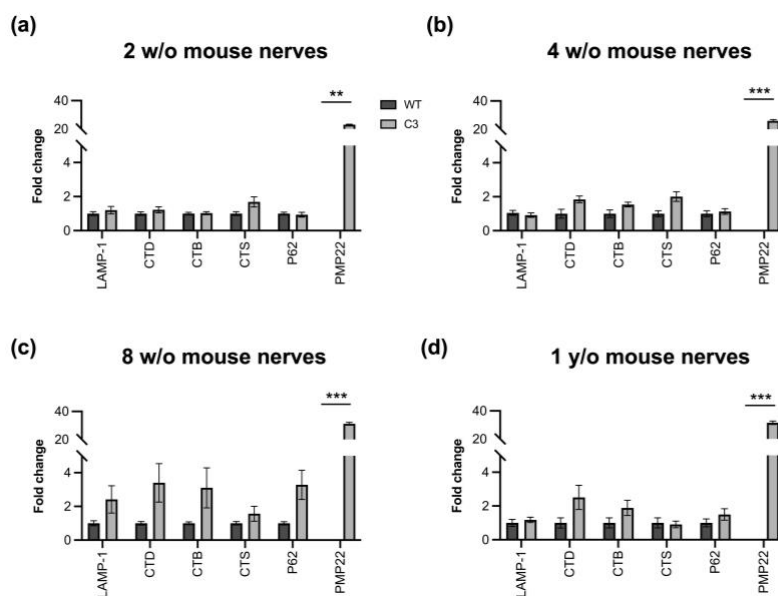


Fig. 1 – Lysosome-associated mRNA expression in the peripheral nerves of (a) two-, (b) four-, and (c) eight-week-old (w/o) and (d) one-year-old (y/o) C3 and WT mice. mRNA was isolated from sciatic and brachial plexus nerves to determine the relative fold changes (FC) of *LAMP-1*, *CTD*, *CTB*, *CTS*, and *P62*. For *PMP22*, Ct values are shown. (a-c) Multiple Mann-Whitney tests with Bonferroni-Dunn correction; (a) $n=4$, (b) $n=8$, (c) $n=6$. (d) Welch's Multiple Unpaired *t*-tests with Bonferroni-Dunn correction; $n=4$. Graphs represent means \pm SEM. ** $p<0.01$; *** $p<0.001$.

2.417-fold (SEM \pm 0.812, $p=0.154$) for *LAMP-1*, by 3.400-fold (SEM \pm 1.140, $p=0.092$) for *CTD*, and by 3.102-fold (SEM \pm 1.186, $p>0.999$) for *CTB*. Meanwhile, *CTS* expression increased by 1.566-fold (SEM \pm 0.444, $p>0.999$). Relative *P62* mRNA expression levels followed these strong trends with a 3.283-fold (SEM \pm 0.868, $p=0.092$) upregulation in C3 mice.

These increasing trends persisted in the peripheral nerves of one-year-old C3 mice for *LAMP-1* (FC=1.164 \pm 0.158, $p>0.999$), *CTD* (FC=2.500 \pm 0.720, $p=0.651$), *CTB* (FC=1.878 \pm 0.453, $p=0.891$), and *P62* (FC=1.486 \pm 0.340, $p>0.999$) (Fig 1d). However, *CTS* expression was slightly downregulated (FC=0.902 \pm 0.196, $p>0.999$) in C3 mouse nerves isolated at this age.

Increased lysosomal proteins in nerve tissue throughout the lifespan of C3 mice - For the evaluation of lysosomal protein and cathepsin levels throughout the lifespan of C3 mice, WB was performed on sciatic and brachial plexus nerve lysates of two-, four-, and eight-week-old and one-year-old C3 versus WT mice (Fig 2, 3).

Glycosylated LAMP-1 protein was observed as two bands at approximately 100 kDa

and 120 kDa, revealing visibly darker bands in C3 mouse nerves than in WT tissue at all included ages (Fig 2a-d). Band intensity was normalized for β -actin, which has a molecular weight of 43 kDa.

At the age of two weeks, LAMP-1 protein levels were significantly higher ($\Delta=1.024 \pm 0.163$, $p=0.005$) in the nerves of C3 mice than in WT animals (Fig 2a, e). Furthermore, four-week-old C3 mice displayed a strong significant 2.275-fold increase in LAMP-1 protein (SEM \pm 0.410, $p<0.001$) (Fig 2b, f), and at the age of eight weeks, significant 1.403-fold increments (SEM \pm 0.310, $p=0.010$) were observed (Fig 2c, g). Finally, one-year-old C3 mice also displayed significant elevations in LAMP-1 levels ($\Delta=0.729 \pm 0.218$, $p=0.027$) compared to WT animals (Fig 2d, h).

Murine CTD bands became visible at approximately 52 kDa, 48 kDa, and 34 kDa, corresponding to pro-CTD, single-chain mature CTD (SS-CTD), and the heavy chain of double-stranded mature CTD (DS-CTD), respectively (Fig 3a-d). Similarly, three CTB bands were visualized at 46 kDa, 31 kDa, and 25 kDa (Fig 3i-l). These bands respectively represented pro-CTB, single-chain CTB (SS-CTB), and the heavy chain of

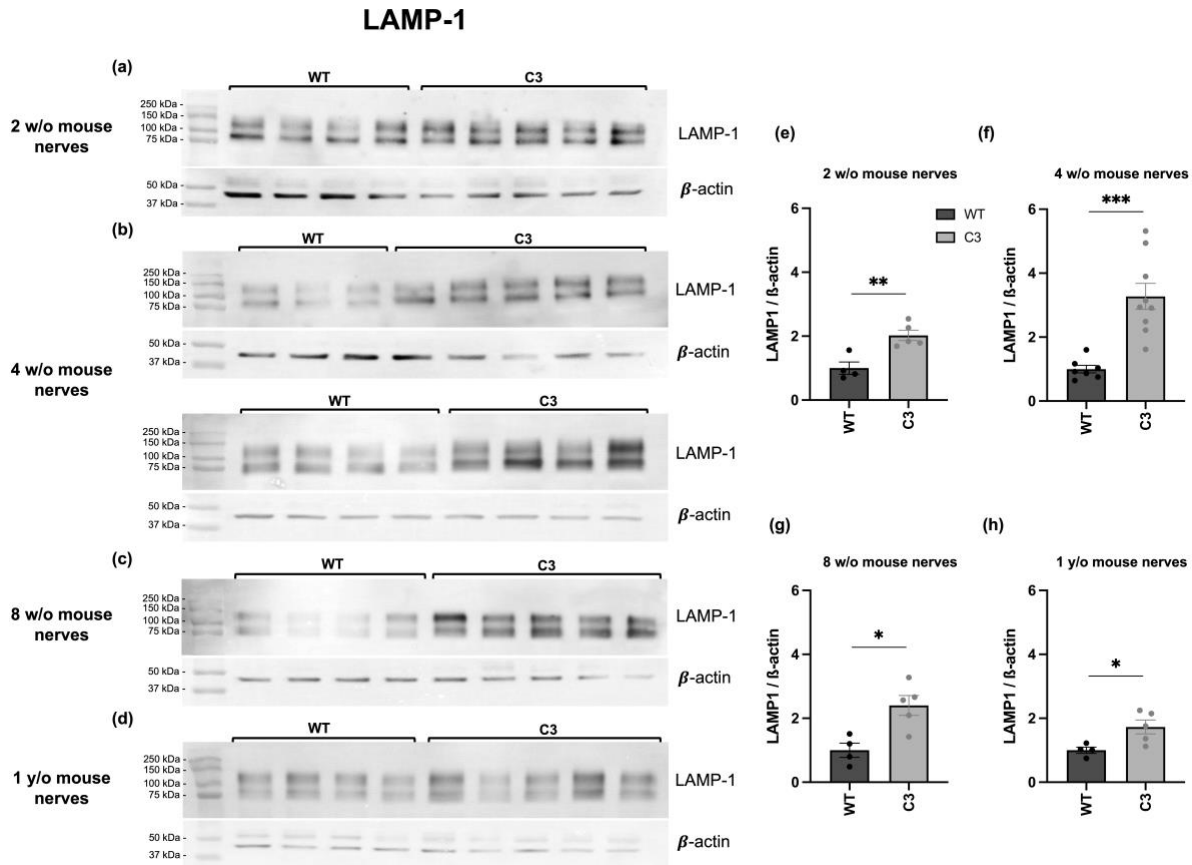


Fig. 2 – LAMP-1 protein levels in C3 mouse nerves compared to WT nerves at the ages of (a, e) two, (b, f) four, and (c, g) eight weeks and (d, h) at one year old. (e-h) LAMP-1 intensity was normalized for the intensity of the reference protein, β -actin. (e, g, h) Unpaired *t*-test, $n=4$; (f) Welch's Unpaired *t*-test, $n=7$. Graphs represent means \pm SEM. * $p < 0.05$; ** $p < 0.01$, *** $p < 0.001$.

double-stranded CTB (DS-CTB). C3 mouse nerves exhibited visually higher band intensities for CTD and CTB at all observed ages.

In two-week-old C3 nerve tissue, all CTD isoforms (pro-CTD: $\Delta=0.505 \pm 0.188$, $p=0.229$; SS-CTD; $\Delta=0.564 \pm 0.131$, $p=0.114$; DS-CTD: $\Delta=0.292 \pm 0.120$, $p=0.800$) and total CTD protein ($\Delta=0.474 \pm 0.099$, $p=0.114$) were slightly increased compared to WT animals (Fig 3a, e). However, pro-CTB ($\Delta=-0.246 \pm 0.102$, $p=0.802$), SS-CTB ($\Delta=-0.013 \pm 0.118$, $p>0.999$), DS-CTB ($\Delta=-0.449 \pm 0.278$, $p>0.999$), and total CTB levels ($\Delta=-0.073 \pm 0.097$, $p>0.999$) were slightly lower in C3 mouse nerves than in WT nerves (Fig 3i, m).

Both cathepsins were strongly elevated in the peripheral nerves of four-week-old C3 mice. At this age, CTD protein was significantly increased by 2.372-fold (SEM ± 0.353 , $p<0.001$) for pro-CTD, 1.879-fold (SEM ± 0.443 , $p=0.010$) for SS-CTD, and 0.671-fold (SEM ± 0.205 , $p=0.047$) for

DS-CTD (Fig 3b, f). Additionally, total CTD levels were significantly elevated by 1.594-fold (SEM ± 0.310 , $p=0.003$) in C3 mice. Similarly, four-week-old C3 mice displayed increasing trends for pro-CTB ($\Delta=0.648 \pm 0.393$, $p=0.719$), SS-CTB ($\Delta=0.505 \pm 0.382$, $p>0.999$), DS-CTB ($\Delta=2.254 \pm 0.578$, $p=0.067$), and total CTB protein ($\Delta=0.834 \pm 0.395$, $p=0.409$) (Fig 3j, n).

Remarkably, all CTD forms were slightly lower in the peripheral nerves of C3 mice at eight weeks of age (Fig 3c, g). Pro-CTD decreased by 0.376-fold (SEM ± 0.103 , $p=0.656$), SS-CTD by 0.256-fold (SEM ± 0.126 , $p>0.999$), DS-CTD by 0.312-fold (SEM ± 0.144 , $p=0.629$), and total CTD by 0.374 (SEM ± 0.082 , $p=0.401$). However, C3 mouse nerves demonstrated a strong 2.333-fold (SEM ± 0.989 , $p=0.254$) increase in pro-CTB (Fig 3k, o). The active CTB forms (SS-CTB: $\Delta=0.515 \pm 0.263$, $p=0.127$; DS-CTB: $\Delta=0.713 \pm 0.381$,

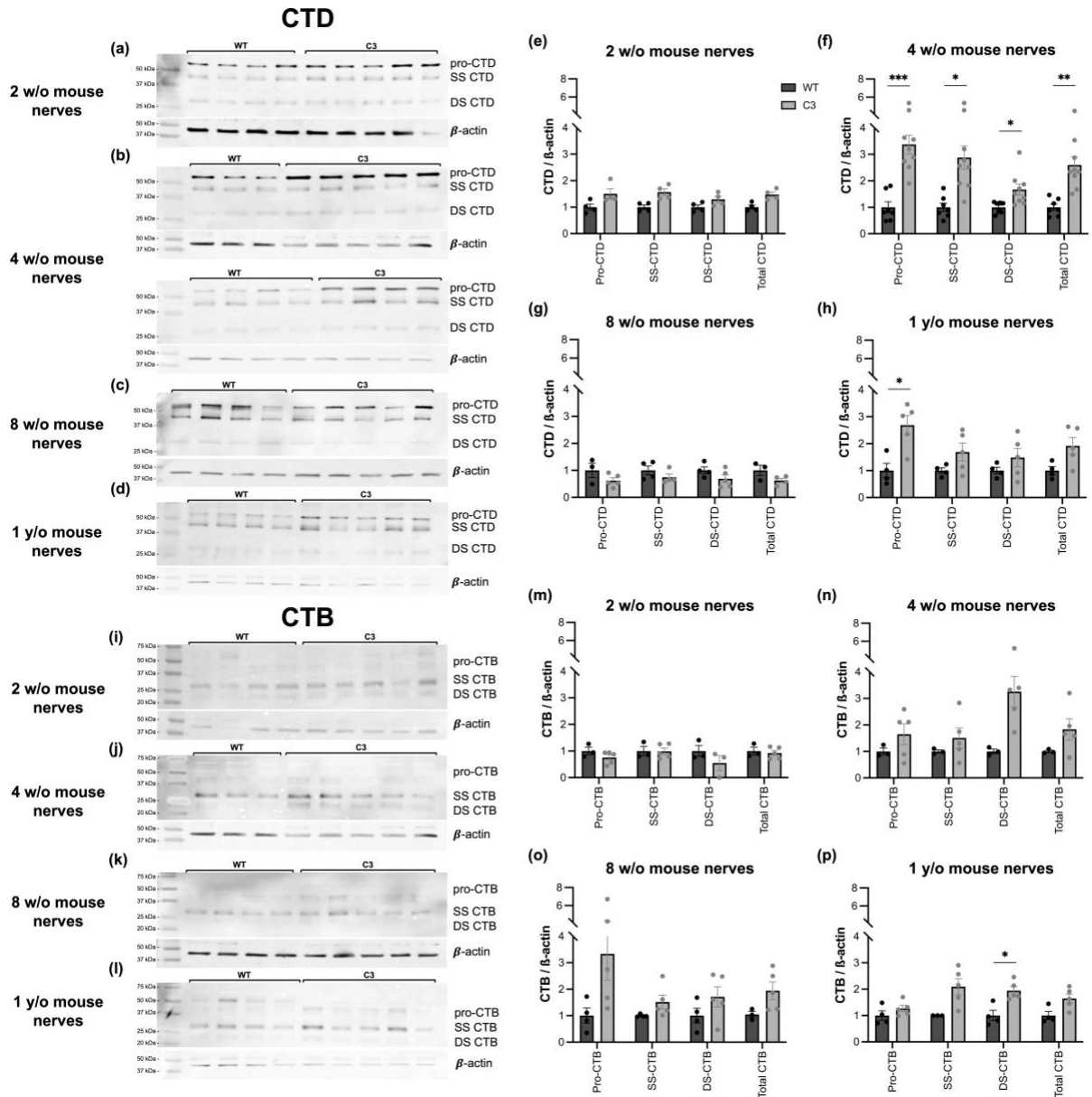


Fig. 3 – Lysosomal cathepsins in the peripheral nerves of C3 mice compared to WT at the ages of (a, e, i, m) two, (b, f, j, n) four, and (c, g, k, o) eight weeks and at (d, h, l, p) one-year old. (a-d) Visualized CTD levels comprised pro-CTD, single chain mature CTD (SS-CTD), and double chain mature CTD (DS-CTD). (i-l) Total CTB levels consisted of pro-CTB, SS-CTB, and DS-CTB. All (e-h) CTD and (m-p) CTB forms were normalized for β -actin. (e, o) Multiple Mann-Whitney tests with Bonferroni-Dunn correction; (e) $n=4$, (o) $n=3$; (f, n, p) Welch's Unpaired Multiple t -tests with Bonferroni-Dunn correction; (f) $n=7$, (n) $n=3$, (p) $n=4$; (g, h, m) Multiple Unpaired t -tests with Bonferroni-Dunn correction; (g, h) $n=4$, (m) $n=3$. Graphs represent means \pm SEM. * $p < 0.05$; ** $p < 0.01$, *** $p < 0.001$.

$p > 0.999$) and ultimately, total CTB ($\Delta = 0.902 \pm 0.332$, $p = 0.286$) followed this increasing trend.

In the nerve tissue of one-year-old C3 mice, pro-CTD was significantly elevated by 1.685-fold (SEM ± 0.364 , $p = 0.038$) (Fig 3d, h). Furthermore,

SS-CTD ($\Delta = 0.690 \pm 0.328$, $p = 0.460$), DS-CTD ($\Delta = 0.484 \pm 0.342$, $p > 0.999$), and total CTD protein ($\Delta = 0.918 \pm 0.311$, $p = 0.178$) revealed increasing trends in C3 mice. In addition, pro-CTB was only slightly elevated by 0.262-fold (SEM ± 0.123 ,

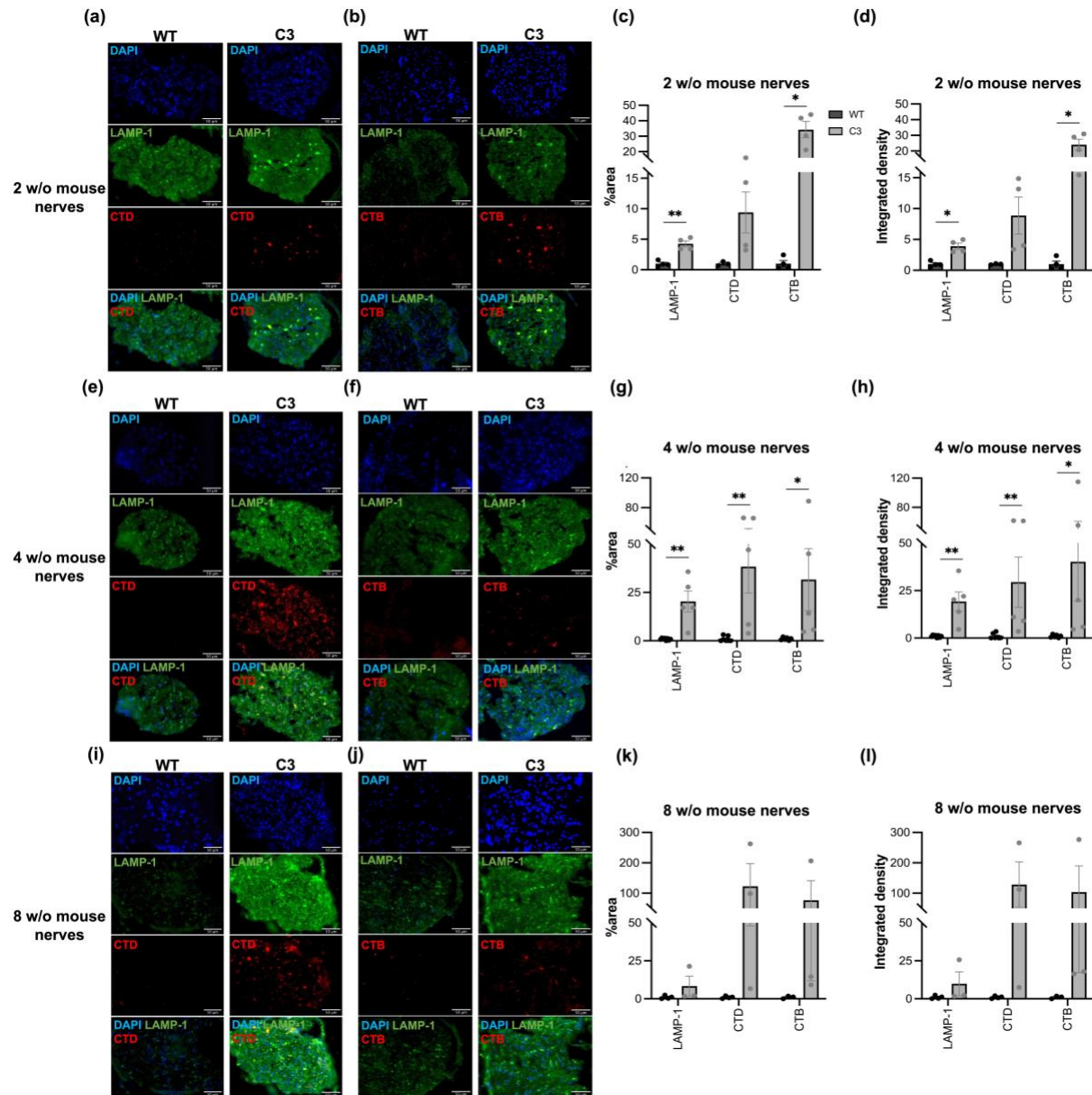


Fig. 4 – Increased lysosomal proteins and cathepsins in C3 sciatic nerves at the ages of (a-d) two, (e-h) four, and (i-l) eight weeks. Sciatic nerves were immunohistochemically stained for (a-b, e-f, i-j) LAMP-1, (a, e, i) CTD, and (b, f, j) CTB. Scale bars: 50 μ m. (c, g, k) %area and (d, h, l) integrated densities were normalized for comparison. (c, d, g, h) Welch's Unpaired Multiple t-tests with Bonferroni-Dunn correction; (c, d) $n=3$, (g, h) $n=5$; (k, l) Multiple Mann-Whitney tests with Bonferroni-Dunn correction; $n=3$. Graphs represent means \pm SEM. * $p < 0.05$; ** $p < 0.01$.

$p > 0.999$), but active SS-CTB and DS-CTB were more strongly increased in these one-year-old C3 nerves, respectively by 1.093-fold (SEM \pm 0.308 $p=0.096$) and 0.942-fold (SEM \pm 0.154 $p=0.036$) with DS-CTB reaching significance (Fig 3l, p). Additionally, total CTB was 0.641-fold (SEM \pm 0.175, $p=0.110$) higher in C3 nerve tissue.

Immunohistochemical confirmation of increased lysosomal proteins in C3 nerve tissue – To visualize and confirm the lysosomal changes on a protein level, we determined the lysosomal protein levels in C3 sciatic nerves using IHC (Fig 4). To do so, sciatic nerve tissue was isolated from C3 and WT animals at the ages of two (Fig 4a-d),

four (Fig 4e-h), and eight weeks (Fig 4i-l) and immunohistochemically prepared to stain LAMP-1, CTD, and CTB. For image quantification, the %area and integrated densities were normalized to display differences (Fig 4c-d, g-h, k-l). Our IHC findings confirmed the elevations of lysosomal protein and cathepsins in two-, four-, and eight-week-old C3 mice.

In two-week-old sciatic nerve tissue, LAMP-1 (Fig 4a-b), CTD (Fig 4a), and CTB (Fig 4b) levels were visibly higher in C3 mice than in WT. Moreover, CTD and CTB visibly overlapped with intense LAMP-1 areas. At this age, LAMP-1 %area ($\Delta=2.905 \pm 0.498, p=0.016$) and integrated density ($\Delta=3.248 \pm 0.483, p=0.009$) were significantly elevated in C3 nerves compared to WT (Fig 4c-d). Furthermore, CTD %area ($\Delta=7.868 \pm 3.000, p=0.236$) and integrated density ($\Delta=8.392 \pm 3.351, p=0.261$) demonstrated strong increasing trends in C3 nerve tissue. Finally, significant increases were observed in CTB %area ($\Delta=22.995 \pm 3.599, p=0.021$) and integrated density ($\Delta=33.288 \pm 5.314, p=0.024$) in two-week-old C3 animals.

At the age of four weeks, LAMP-1 (Fig 4e-f), CTD (Fig 4e), and CTB (Fig 4f) protein elevations in C3 mice were reinforced, displaying similar overlapping patterns of LAMP-1 with both cathepsins. Moreover, C3 sciatic nerves displayed significant increases in the %area (Fig 4g) and integrated densities (Fig 4h) of LAMP-1 (respectively $\Delta=19.457 \pm 5.379, p=0.005$; and $\Delta=18.249 \pm 5.066, p=0.005$), CTD (respectively $\Delta=37.295 \pm 13.600, p=0.008$; and $\Delta=28.427 \pm 13.238, p=0.008$), and CTB (respectively $\Delta=30.616 \pm 16.030, p=0.013$; and $\Delta=39.180 \pm 20.827, p=0.013$) compared to WT mice.

In eight-week-old nerve tissue, LAMP-1 (Fig 4i-j), CTD (Fig 4i), and CTB (Fig 4j) were visibly elevated in C3 compared to nerves from WT animals. Similar to the other monitored ages, high LAMP-1 intensity was visibly associated with CTD and CTB spots. LAMP-1 %area ($\Delta=7.380 \pm 6.516, p=0.686$) and integrated density ($\Delta=8.880 \pm 7.911, p=0.686$) were increased in C3 mice compared to WT (Fig 4k-l), but to a lesser degree than at four weeks of age (Fig 4g-h). Meanwhile, CTD and CTB %area increased respectively by 121.714-fold

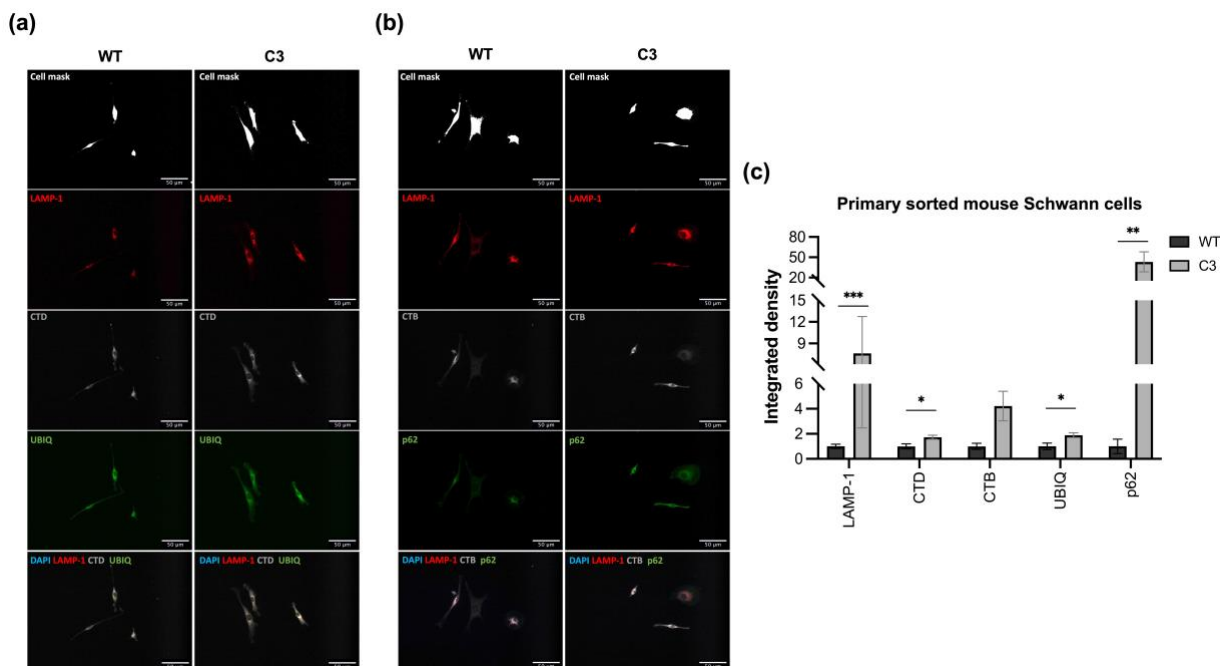


Fig. 5 – Lysosome-associated protein increases in FACS-sorted primary C3 mouse Schwann cells. Primary Schwann cells from C3 and WT mice were isolated and sorted by FACS to obtain CD90.2⁺ pure Schwann cell populations for ICC against (a-b) LAMP-1, (a) CTD, (b) CTB, (a) UBIQ, and (b) p62 proteins. Scale bars: 50 μm. (c) Integrated densities were normalized. *Multiple Mann-Whitney tests with Bonferroni-Dunn correction; n=11.* Graphs represent means \pm SEM. * $p < 0.05$; ** $p < 0.01$ *** $p < 0.001$.

(SEM \pm 74.810, $p=0.171$) and 75.683-fold (SEM \pm 64,822, $p=0.300$), reaching peak protein levels. The same was true for CTD and CTB integrated densities, which were respectively 127.398-fold (SEM \pm 74.906, $p=0.171$) and 102.587-fold (SEM \pm 86.433, $p=0.300$) higher in C3 sciatic nerves compared to WT nerves.

Increasing lysosome-associated proteins in a pure C3 primary mouse Schwann cell population – To evaluate lysosomal changes on a cellular level, we analyzed lysosome-related protein levels in pure primary mouse Schwann cells using ICC (Fig 5). For this purpose, C3 and WT Schwann cell populations were harvested from the sciatic and brachial plexus nerves and sorted by FACS to obtain purified CD90.2⁺ Schwann cell populations. FACS sorted primary Schwann cells with a 95% efficiency. Results obtained from these primary C3 mouse Schwann cells confirmed the elevations in lysosome-related proteins observed in C3 mouse nerve tissue.

In this pure primary Schwann cell population, LAMP-1 levels were visibly higher and more

widespread in C3 compared to WT mice (Fig 5a-b). Similarly, higher intensities were observed for CTD (Fig 5a), CTB (Fig 5b), ubiquitin (UBIQ) (Fig 5a), and p62 proteins (Fig 5b). LAMP-1 integrated density was significantly increased by 6.614-fold (SEM \pm 5.139, $p<0.001$) in the C3 primary Schwann cell population (Fig 5c). Additionally, CTD protein was significantly elevated ($\Delta=0.725 \pm 0.169$, $p=0.043$) in pure C3 Schwann cells, and CTB followed a similar increasing trend ($\Delta=3.213 \pm 1.180$, $p=0.416$). Furthermore, UBIQ ($\Delta=0.894 \pm 0.195$, $p=0.038$) and p62 ($\Delta=42.229 \pm 14.805$, $p=0.001$) protein levels were significantly higher in C3 primary mouse Schwann cells than in WT cells.

Validation of lysosomal increases in a human patient-in-a-dish model for CMT1A – To validate our results in a human-specific CMT1A model, we evaluated the lysosomal-related changes in a human patient-in-a-dish model (Fig 6). We assessed the relative mRNA expression patterns of lysosomal markers in CMT1A patient-derived iPSC (Fig 6a) and differentiated these cells into iPSC-SCP (Fig

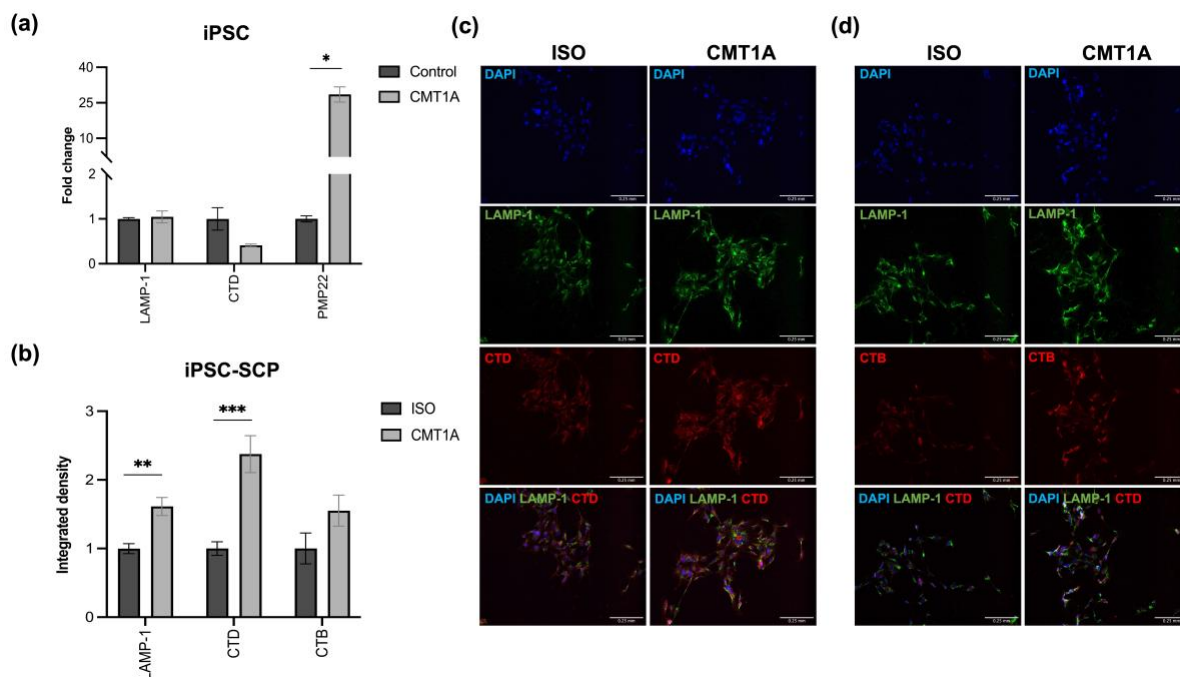


Fig. 6 – Validation of lysosomal proteins and cathepsins in a human patient-in-a-dish model. **(a)** Relative *LAMP-1*, *CTD*, and *PMP22* mRNA expression levels in patient-derived iPSC and healthy control cells. **(b-d)** *LAMP-1*, **(b, c)** *CTD*, and **(b, d)** *CTB* protein levels in Schwann cell precursors derived from CMT1A patient-derived iPSC (iPSC-SCP) and isogenic control cells (ISO). Scale bars: 0.25 mm. **(b)** Integrated densities were normalized. **(a)** Welch's Multiple *t*-tests with Bonferroni-Dunn correction, $n=4$; **(b)** Multiple Mann-Whitney tests with Bonferroni-Dunn correction; $n=13$. ICC experiment was performed in duplicate. Graphs represent means \pm SEM. * $p<0.05$ ** $p<0.01$, *** $p<0.001$.

6b-d) to function as a human patient-in-a-dish model for CMT1A. Our results from this human *in vitro* model confirmed the elevated lysosomal protein and cathepsin levels observed in C3 mice.

The CMT1A genotype of patient-derived iPSC colonies was confirmed by the significantly elevated *PMP22* expression levels in comparison to control cells (FC=27.536 ± 3.219, *p*=0.010) (**Fig 6a**). Furthermore, CMT1A iPSC cells demonstrated slight increases in relative *LAMP-1* expression (FC=0.045 ± 0.132, *p*>0.999), but decreases in *CTD* mRNA levels (FC=-0.588 ± 0.030, *p*=0.192).

Moreover, differentiated iPSC-SCP from CMT1A patients had visually higher levels of LAMP-1 (**Fig 6c-d**), CTD (**Fig 6c**), and CTB (**Fig 6d**). Additionally, it appeared that CTD and CTB overlapped with LAMP-1-intense cell portions. LAMP-1 protein significantly increased by 0.613-fold (SEM ± 0.132, *p*=0.001) in CMT1A iPSC-SCP compared to isogenic iPSC-SCP, in which the *PMP22* duplication was repaired (**Fig 6b**). Additionally, CTD was significantly elevated by 1.375-fold (SEM ± 0.268, *p*<0.001) in CMT1A cells, while CTB revealed an increasing trend (Δ =0.551 ± 0.227, *p*=0.099).

DISCUSSION

Lysosome-related alterations over the lifespan of the C3 CMT1A mouse model – The aggregation of misfolded PMP22 severely impairs protein degradation mechanisms in CMT1A and has been suggested to involve the autophagy-dependent lysosomal pathway (12, 40-42). Previous research has demonstrated that upregulated lysosomes and autophagosomes clear PMP22 upon the failure of proteasomal degradation in CMT1A (10, 12, 40, 41, 43). As these studies were based on research models with more severe phenotypes, such as the C22 mice model (10, 12), it is necessary to confirm lysosomal changes in more translatable CMT1A models, such as the C3 mouse model (35, 36). These transgenic *PMP22*-overexpressing mice progressively develop mild neuromuscular impairments and are described to be more similar to human pathology (44). To fully characterize lysosomal alterations in the progressive CMT1A C3 mice model, mRNA and protein changes were monitored at different stages of the mouse lifespan (**Fig 7**). To our knowledge, we are the first to perform an in-depth analysis of lysosomal-related changes in CMT1A.

At the mRNA level, we determined the relative expression of *LAMP-1*, *CTD*, *CTB*, *CTS*, and *P62* in two-, four- and eight-week-old, and one-year-old C3 mice *versus* WT animals to evaluate lysosomal changes over time.

LAMP-1 is the major glycosylated protein of the lysosomal membrane and is, therefore, routinely used as a lysosomal marker (45). Our results demonstrated elevated *LAMP-1* mRNA levels in C3 nerve tissue at the ages of two weeks, eight weeks, and one year, with a slight decrease being observed in four-week-old mice. These increasing trends suggest transcriptional lysosomal upregulation over the lifespan of the C3 mouse model.

CTD and **CTB** are aspartic and cysteine cathepsin proteases, respectively (13). *CTD* mRNA levels displayed the greatest differences among all monitored lysosomal genes. *CTD* expression became upregulated at the age of two weeks, further increasing at four weeks and peaking at eight weeks with a 3.4-fold increase. In one-year-old C3 nerves, relative *CTD* levels were still 2.5-fold higher compared to WT tissue. Relative mRNA expression levels of *CTB* followed the same age-dependent increases as *CTD* in C3 mice, reaching considerably higher levels than WT littermates. In eight-week-old C3 mice, *CTB* level peaked with a 3.1-fold overexpression. These substantial increases throughout the lifespan of the C3 mice indicate that CTD and CTB are involved in CMT1A pathology.

CTS is a lysosomal cysteine cathepsin with limited tissue expression that is linked to immune cells, including macrophages (46). Our results show a trend of increased *CTS* expression in two-, four-, and eight-week-old C3 mice. Surprisingly, *CTS* levels were slightly downregulated in one-year-old C3 *versus* WT animals. These findings are entirely novel since CTS has never been investigated before in CMT1A. This enzyme's unique macrophagic expression profile suggests its association with the secondary immune response in CMT1A, which is characterized by lymphocytic infiltration and the presence of demyelination-associated macrophages in the peripheral nerves (10, 47, 48). Moreover, the therapeutic reduction of macrophages in CMT1A mouse pups improved the Schwann cell phenotype and resulted in motor function preservation (49). Hence, we propose CTS as an attractive CMT1A target for further investigation.

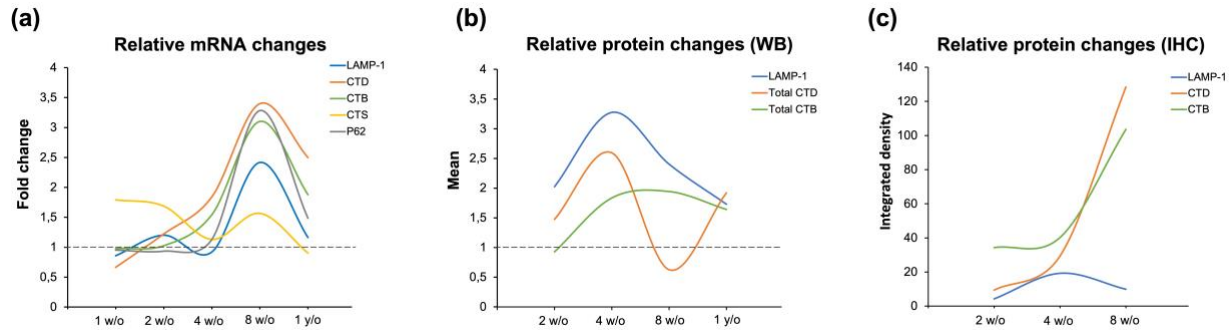


Fig. 7 – Relative lysosomal-related changes in (a) mRNA and (b, c) protein levels observed throughout the lifespan of C3 *versus* WT mice. Graphs represent (a) fold changes, (b) WB means normalized for β -actin, and (c) IHC mean integrated densities relative to WT animals. (a-b) Dashed lines represent FC/mean=1, and values above the lines represent upregulation in C3 animals compared to WT mice.

The **p62** protein is an autophagy adaptor targeting misfolded proteins towards the lysosomal-autophagic pathway (50, 51). Therefore, we monitored *P62* expression levels to assess autophagic activation in CMT1A. We successfully discovered *P62* mRNA upregulation in the nerves of C3 mice at the ages of four weeks, eight weeks, and one year. Although previous papers only evaluated protein levels, similar increases in autophagic proteins, including p62, autophagy-related 7 (*Atg7*), and microtubule-associated protein light chain 3 (*LC3*), were observed in the peripheral nerves of one-year-old C22 mice (10). Additionally, Fortun et al. reported *Atg7* protein elevation in C22 mice at three weeks old (12).

Altogether, our mRNA data demonstrated the transcriptional upregulation of the lysosomal-autophagic pathway over the lifespan of a highly representative CMT1A animal model, strongly suggesting lysosomal involvement in CMT1A development and progression.

At a protein level, we monitored lysosomal LAMP-1, CTD, and CTB levels in the peripheral nerve tissue of C3 mice throughout their lifespan. Thereby, the lysosomal changes in the C3 mouse model were completely characterized.

LAMP-1 protein levels were significantly increased in C3 mice at all observed ages, as confirmed by WB and IHC. Peak upregulation was observed in four-week-old C3 tissue, presenting a 2.7-fold elevation compared to WT mice according to WB data. Earlier studies have reported 3-to 5-fold increases in LAMP-1 protein in association with PMP22 in the sciatic nerves of six-month-old

C22 mice (12). Chittoor et al. further confirmed LAMP-1 elevations in C22 mice at the ages of two months, six months, and one year (10). LAMP-1 upregulation and PMP22 co-localization were also described in Trembler J mice at the age of one year (15) and at unspecified adult age (40). Hence, our results are in line with existing research, confirming lysosomal upregulation over the lifespan of the C3 mouse model.

Interestingly, C3 mice displayed greater increases at the protein level than at the mRNA level at all monitored ages. In addition, LAMP-1 protein levels peaked in the nerves of four-week-old C3 mice, but mRNA levels revealed a decreasing trend at this age. Such differences can be explained by the severely disrupted proteostasis in CMT1A. Hence, an impaired degradation of LAMP-1 protein causes levels to build up over time (10), independent of protein transcription.

CTD protein elevations were observed in C3 mouse nerve tissue at all monitored ages. Data from WB and IHC consistently demonstrated substantial CTD increases in C3 mice at the ages of two weeks, four weeks, and one year. Nevertheless, at eight weeks old, WB data suggested CTD levels to be slightly lower than in WT nerves. Contrarily, IHC data indicated that CTD protein elevations peak in C3 nerves at this age. Yet, it is interesting to mention that without the removal of a statistical outlier of the eight-week-old C3 mice, a slight increase was detected in pro-CTD and total CTD by WB data (data not shown). Moreover, differences between both techniques are possible due to sample preparation, but it is more likely that variances in the β -actin reference protein are responsible for the

observed WB decreases. Several blots displayed non-constitutive expression of β -actin, indicating that this protein is not the best reference protein for CMT1A nerves. For a more reliable analysis, WB experiments should be repeated with a more stable reference protein.

All CTD isoforms were upregulated in C3 mice at two weeks, four weeks, and one year of age. However, although differences could not be observed at two weeks, four-week-and one-year-old C3 animals exhibited the most notable increases in pro-CTD. Meanwhile, DS-CTD displayed the smallest increments throughout the lifespan of the mice. Consistently higher pro-CTD levels may result from impaired CTD processing or proteolysis defects, as this was also suggested in the C22 model (10). In these C22 mice, the ratio of active-/pro-CTD was reported to remain steady over the ages of two months, six months, and one year, while the ratio increased in an age-dependent manner in WT nerves (10). Nevertheless, it needs to be mentioned that the researchers of this study identified pro-CTD at 48 kDa while reporting only one active CTD isoform at 28 kDa. Similarly, increased levels of pro-CTD, identified at 48 kDa, and mature CTD, identified at 34 kDa, were reported in the nerves of adult Trembler J mice (40). Although we also observed mature DS-CTD at 34 kDa, we identified the 48 kDa band as an active intermediate SS-CTD isoform and defined pro-CTD bands at 52 kDa, based on consistent descriptions in literature (24, 52, 53). Hence, lysosomal CTD elevations have been reported in other CMT1A models, but discussions about the distinct isoforms are restrained by inconsistent identifications.

CTB protein levels were increased over the lifespan of C3 mice, but discrepancies were observed between both detection techniques. While IHC data demonstrated strong significant CTB elevations in two-week-old C3 mice, WB suggested slight CTB protein decreases at this age. As described above, this is likely caused by inconsistent β -actin expression. At all other included ages, mice exhibited increases in all CTB isoforms and total CTB, with both techniques reporting peak upregulation in eight-week-old C3 mice. Meanwhile, the strongest elevations were observed in DS-CTB in four-week-old mice, in pro-CTB in eight-week-old animals, and both in SS-CTB and DS-CTB in one-year-old C3 mice.

Due to the lack of distinct trends and inconsistencies in isoform identification, as exposed for CTD, it is particularly difficult to draw conclusions about the various enzymatic forms of cathepsins. Interpretation is even further complicated by slight differences in functions and activities of the enzymatically different forms of CTD, and likely CTB, which might also depend on the pH level (24). Therefore, it would be interesting to take a more detailed look into the various enzymatic forms of CTD and CTB in CMT1A, using highly sensitive techniques, such as gelatin zymography, that better discern cathepsin molecular weights, activities, and posttranslational modifications (54). Additionally, such methods would allow the determination of the light chains of DS-CTD and DS-CTB, which are challenging to detect by WB due to their small sizes of 14 kDa (24) and 5 kDa (25), respectively.

Confirmation of compensatory lysosomal upregulation in pure primary isolated Schwann cells from C3 mice – Previous studies have assessed lysosomal-autophagic changes in primary Schwann cell populations from C22 (12) and Trembler J mice (41) but did not take fibroblast contamination into account. Hence, we aimed to confirm the upregulation of lysosomal-related proteins in a pure primary Schwann cell population harvested from C3 nerve tissue, using FACS sorting to eliminate fibroblasts with a 95% efficiency.

Our data confirm lysosomal and autophagic protein upregulation in C3 CMT1A Schwann cells by detecting increases in LAMP-1, CTD, CTB, p62, and UBIQ. These data are consistent with our previous findings in C3 nerve tissue and, moreover, support previous research where autophagic upregulation was also reported in non-purified primary Schwann cells from C22 mice (12) and Trembler J mice (41). Furthermore, lysosomal upregulation and degradation of PMP22 were reported in a healthy rat Schwann cell line upon treatment with a proteasome inhibitor, also increasing the number and size of autophagosomes (41). Altogether, these results provide strong evidence for the lysosomal-autophagic activation upon UPS overload in Schwann cells affected by CMT1A. However, further research should assess the mRNA expression of more UPS, autophagic, and lysosomal markers to unravel the exact mechanisms of this compensatory feedback system.

Validation of lysosomal upregulation in a patient-in-a-dish model – We aimed to validate the lysosomal upregulation in a human-specific Schwann cell model to increase clinical translatability. A similar study has been performed using dermal fibroblasts from CMT1A patients as these cells also express *PMP22*, making them suitable for studying CMT1A pathology (43). However, Schwann cells are the primary affected cells in CMT1A since they express the strong Schwann cell-specific P1 *PMP22* promoter, which is absent in all other cell types (7). Hence, our human model based on CMT1A iPSC-SCP is more representable for disease studies.

Increased LAMP-1 levels were confirmed at the mRNA and the protein level in CMT1A-derived iPSC-SCs. The 1.5-fold LAMP-1 protein increase in our patient-derived iPSC-SCP is in line with the 1.5-fold LAMP-1 elevation observed in patient-derived dermal fibroblasts (43). Interestingly, these CMT1A fibroblasts also demonstrated p62 and LC3 protein increases and LC3-PMP22 colocalization, confirming autophagic upregulation in a human CMT1A model. These findings are consistent with our data from the C3 mouse model and, hence, indicate that further elucidating autophagic upregulation in human *in vitro* models will be necessary for future research.

Interestingly, CTD mRNA expression followed a decreasing trend in CMT1A patient-derived iPSC compared to healthy control cells, while significant CTD protein elevations were confirmed in these cells after differentiation into Schwann cell precursors. Furthermore, increased CTB protein levels were observed in patient-derived iPSC-SCP, in agreement with our findings in the C3 mouse model.

The observed discrepancy between CTD mRNA and protein expression might be explained by the failure of CTD protein degradation in CMT1A. Moreover, differences can also be present before and after the differentiation into iPSC-SCP, which evokes considerably higher *PMP22* levels due to the expression of the powerful P1 promoter (7). Nevertheless, the experiment should be repeated to exclude experimental bias.

Furthermore, it must be mentioned that this iPSC-derived patient-in-a-dish model is limited by a lack of maturation of the iPSC-SCP, failing to recapitulate the fully mature functional Schwann cell phenotype (33). Hence, it is required to

thoroughly validate the patient-derived iPSC-SC model, as well as other human-specific models, to build more reliable clinical translatability.

Conclusion and future perspectives – Our results provide substantial evidence for the compensatory lysosomal upregulation following *PMP22* misfolding and aggregation throughout different disease phases of CMT1A. Nevertheless, the increasing number of *PMP22* aggregates saturates the activated lysosomes and autophagosomes, hence, accumulating within these organelles (15). We suggest that the lysosomal accumulation of *PMP22* contributes to CMT1A development and progression, presumably through the aberrant increase of lysosomal CTD and CTB.

Increased cytosolic cathepsin levels can induce severe cellular damage and apoptosis (19, 20). Although findings related to CMT1A Schwann cell apoptosis are contradictory, Schwann cell apoptosis has been demonstrated in patient nerve biopsies and *PMP22*-overexpressing animal models (55, 56). Hence, future research should address the role of cathepsins in Schwann cell apoptosis and proliferation.

In addition, extracellular secretion of CTD and CTB can lead to the degradation of essential ECM proteins, including collagen type IV and laminin (26, 28). Even though it remains to be proven that extracellular CTD and CTB levels are increased in CMT1A, a fascinating link can be made between the extracellular release of lysosomal cathepsins and phenotypic Schwann cell alterations observed in CMT1A studies (6, 9, 57)

Hence, although further research should assess the exact role of these cathepsins in CMT1A, we suggest selective CTD and CTB inhibitors as promising candidate drugs for CMT1A (13).

CONCLUSION

Our results demonstrated lysosomal and autophagic upregulation over the lifespan of the representative C3 mouse model for CMT1A. Further evidence validated these lysosome-related increases in pure primary Schwann cells from C3 mice and in Schwann cell precursors obtained from patient-derived iPSC differentiation. In addition, CTD and CTB were substantially elevated over the lifespan of C3 mice, in pure C3 primary mouse Schwann cell cultures, and in CMT1A iPSC-SCP. Hence, we suggest selective CTD and CTB inhibitors as promising drugs for CMT1A patients.

REFERENCES

1. Pareyson D, Marchesi C. Diagnosis, natural history, and management of Charcot-Marie-Tooth disease. *Lancet Neurol.* 2009;8(7):654-67.
2. van Paassen BW, van der Kooi AJ, van Spaendonck-Zwarts KY, Verhamme C, Baas F, de Visser M. PMP22 related neuropathies: Charcot-Marie-Tooth disease type 1A and Hereditary Neuropathy with liability to Pressure Palsies. *Orphanet J Rare Dis.* 2014;9:38.
3. Bird TD. Charcot-Marie-Tooth (CMT) Hereditary Neuropathy Overview. In: Adam MP, Ardinger HH, Pagon RA, Wallace SE, Bean LJH, Mirzaa G, et al., editors. *GeneReviews*((R)). Seattle (WA)1993, Revised: 2021.
4. NIH. Charcot-Marie-Tooth Disease Fact Sheet: National Library of Medicine, NIH; 2018 [updated 2021-11-15. Available from: <https://www.ninds.nih.gov/Disorders/Patient-Caregiver-Education/Fact-Sheets/Charcot-Marie-Tooth-Disease-Fact-Sheet>.
5. Hanemann CO, Muller HW. Pathogenesis of Charcot-Marie-Tooth 1A (CMT1A) neuropathy. *Trends Neurosci.* 1998;21(7):282-6.
6. Niemann A, Berger P, Suter U. Pathomechanisms of mutant proteins in Charcot-Marie-Tooth disease. *Neuromolecular Med.* 2006;8(1-2):217-42.
7. Marinko JT, Carter BD, Sanders CR. Direct relationship between increased expression and mistrafficking of the Charcot-Marie-Tooth-associated protein PMP22. *Journal of Biological Chemistry.* 2020;295(34):11963-70.
8. Notterpek L, Ryan MC, Tobler AR, Shooter EM. PMP22 accumulation in aggresomes: implications for CMT1A pathology. *Neurobiol Dis.* 1999;6(5):450-60.
9. Hanemann CO, Gabreels-Festen AA, Stoll G, Muller HW. Schwann cell differentiation in Charcot-Marie-Tooth disease type 1A (CMT1A): normal number of myelinating Schwann cells in young CMT1A patients and neural cell adhesion molecule expression in onion bulbs. *Acta Neuropathol.* 1997;94(4):310-5.
10. Chittoor VG, Sooyeon L, Rangaraju S, Nicks JR, Schmidt JT, Madorsky I, et al. Biochemical characterization of protein quality control mechanisms during disease progression in the C22 mouse model of CMT1A. *ASN Neuro.* 2013;5(5):e00128.
11. Schleich JP, Narayan M, Alford C, Mittendorf KF, Carter BD, Li J, et al. Conformational Stability and Pathogenic Misfolding of the Integral Membrane Protein PMP22. *J Am Chem Soc.* 2015;137(27):8758-68.
12. Fortun J, Go JC, Li J, Amici SA, Dunn WA, Jr., Notterpek L. Alterations in degradative pathways and protein aggregation in a neuropathy model based on PMP22 overexpression. *Neurobiol Dis.* 2006;22(1):153-64.
13. Yadati T, Houben T, Bitorina A, Shiri-Sverdlov R. The Ins and Outs of Cathepsins: Physiological Function and Role in Disease Management. *Cells.* 2020;9(7).
14. Tancini B, Buratta S, Delo F, Sagini K, Chiaradia E, Pellegrino RM, et al. Lysosomal Exocytosis: The Extracellular Role of an Intracellular Organelle. *Membranes (Basel).* 2020;10(12).
15. Fortun J, Dunn WA, Jr., Joy S, Li J, Notterpek L. Emerging role for autophagy in the removal of aggresomes in Schwann cells. *J Neurosci.* 2003;23(33):10672-80.
16. Gabande-Rodriguez E, Boya P, Labrador V, Dotti CG, Ledesma MD. High sphingomyelin levels induce lysosomal damage and autophagy dysfunction in Niemann Pick disease type A. *Cell Death Differ.* 2014;21(6):864-75.
17. Boya P, Andreau K, Poncet D, Zamzami N, Perfettini JL, Metivier D, et al. Lysosomal membrane permeabilization induces cell death in a mitochondrion-dependent fashion. *J Exp Med.* 2003;197(10):1323-34.
18. Yang AJ, Chandswangbhuvana D, Margol L, Glabe CG. Loss of endosomal/lysosomal membrane impermeability is an early event in amyloid Abeta1-42 pathogenesis. *J Neurosci Res.* 1998;52(6):691-8.

19. Freeman D, Cedillos R, Choyke S, Lukic Z, McGuire K, Marvin S, et al. Alpha-synuclein induces lysosomal rupture and cathepsin dependent reactive oxygen species following endocytosis. *PLoS One*. 2013;8(4):e62143.
20. Wang F, Gomez-Sintes R, Boya P. Lysosomal membrane permeabilization and cell death. *Traffic*. 2018;19(12):918-31.
21. Bunk J, Prieto Huarcaya S, Drobny A, Dobert JP, Walther L, Rose-John S, et al. Cathepsin D Variants Associated With Neurodegenerative Diseases Show Dysregulated Functionality and Modified alpha-Synuclein Degradation Properties. *Front Cell Dev Biol*. 2021;9:581805.
22. Fonovic M, Turk B. Cysteine cathepsins and extracellular matrix degradation. *Biochim Biophys Acta*. 2014;1840(8):2560-70.
23. Almeida PC, Nantes IL, Chagas JR, Rizzi CC, Faljoni-Alario A, Carmona E, et al. Cathepsin B activity regulation. Heparin-like glycosaminoglycans protect human cathepsin B from alkaline pH-induced inactivation. *J Biol Chem*. 2001;276(2):944-51.
24. Benes P, Vetvicka V, Fusek M. Cathepsin D--many functions of one aspartic protease. *Crit Rev Oncol Hematol*. 2008;68(1):12-28.
25. Cavallo-Medved D, Moin K, Sloane B. Cathepsin B: Basis Sequence: Mouse. *AFCS Nat Mol Pages*. 2011;2011:A000508.
26. Patel S, Homaei A, El-Seedi HR, Akhtar N. Cathepsins: Proteases that are vital for survival but can also be fatal. *Biomed Pharmacother*. 2018;105:526-32.
27. Sun H, Lou X, Shan Q, Zhang J, Zhu X, Zhang J, et al. Proteolytic characteristics of cathepsin D related to the recognition and cleavage of its target proteins. *PLoS One*. 2013;8(6):e65733.
28. Vizovisek M, Fonovic M, Turk B. Cysteine cathepsins in extracellular matrix remodeling: Extracellular matrix degradation and beyond. *Matrix Biol*. 2019;75-76:141-59.
29. Chernousov MA, Yu WM, Chen ZL, Carey DJ, Strickland S. Regulation of Schwann cell function by the extracellular matrix. *Glia*. 2008;56(14):1498-507.
30. Podratz JL, Rodriguez E, Windebank AJ. Role of the extracellular matrix in myelination of peripheral nerve. *Glia*. 2001;35(1):35-40.
31. Palumbo C, Massa R, Panico MB, Di Muzio A, Sinibaldi P, Bernardi G, et al. Peripheral nerve extracellular matrix remodeling in Charcot-Marie-Tooth type I disease. *Acta Neuropathol*. 2002;104(3):287-96.
32. Oka N, Kawasaki T, Unuma T, Shigematsu K, Sugiyama H. Different profiles of onion bulb in CIDP and CMT1A in relation to extracellular matrix. *Clin Neuropathol*. 2013;32(5):406-12.
33. Juneja M, Burns J, Saporta MA, Timmerman V. Challenges in modelling the Charcot-Marie-Tooth neuropathies for therapy development. *Journal of Neurology, Neurosurgery & Psychiatry*. 2019;90(1):58.
34. Misko A, Ferguson T, Notterpek L. Matrix metalloproteinase mediated degradation of basement membrane proteins in Trembler J neuropathy nerves. *J Neurochem*. 2002;83(4):885-94.
35. Huxley C, Passage E, Manson A, Putzu G, Figarella-Branger D, Pellissier JF, et al. Construction of a mouse model of Charcot-Marie-Tooth disease type 1A by pronuclear injection of human YAC DNA. *Hum Mol Genet*. 1996;5(5):563-9.
36. Fledrich R, Stassart RM, Sereda MW. Murine therapeutic models for Charcot-Marie-Tooth (CMT) disease. *British Medical Bulletin*. 2012;102(1):89-113.
37. Shi L, Huang L, He R, Huang W, Wang H, Lai X, et al. Modeling the Pathogenesis of Charcot-Marie-Tooth Disease Type 1A Using Patient-Specific iPSCs. *Stem Cell Reports*. 2018;10(1):120-33.
38. Stratton JA, Kumar R, Sinha S, Shah P, Stykel M, Shapira Y, et al. Purification and Characterization of Schwann Cells from Adult Human Skin and Nerve. *eNeuro*. 2017;4(3).
39. Andersen ND, Monje PV. Isolation, Culture, and Cryopreservation of Adult Rodent Schwann Cells Derived from Immediately Dissociated Teased Fibers. *Methods Mol Biol*. 2018;1739:49-66.

40. Notterpek L, Shooter EM, Snipes GJ. Upregulation of the endosomal-lysosomal pathway in the trembler-J neuropathy. *The Journal of neuroscience : the official journal of the Society for Neuroscience*. 1997;17(11):4190-200.
41. Fortun J, Verrier JD, Go JC, Madorsky I, Dunn WA, Notterpek L. The formation of peripheral myelin protein 22 aggregates is hindered by the enhancement of autophagy and expression of cytoplasmic chaperones. *Neurobiology of disease*. 2007;25(2):252-65.
42. Chittoor VG, Sooyeon L, Rangaraju S, Nicks JR, Schmidt JT, Madorsky I, et al. Biochemical characterization of protein quality control mechanisms during disease progression in the C22 mouse model of CMT1A. *ASN neuro*. 2013;5(5):e00128-e.
43. Lee S, Bazick H, Chittoor-Vinod V, Al Salihi MO, Xia G, Notterpek L. Elevated Peripheral Myelin Protein 22, Reduced Mitotic Potential, and Proteasome Impairment in Dermal Fibroblasts from Charcot-Marie-Tooth Disease Type 1A Patients. *Am J Pathol*. 2018;188(3):728-38.
44. Verhamme C, King RH, ten Asbroek AL, Muddle JR, Nourallah M, Wolterman R, et al. Myelin and axon pathology in a long-term study of PMP22-overexpressing mice. *J Neuropathol Exp Neurol*. 2011;70(5):386-98.
45. Cheng XT, Xie YX, Zhou B, Huang N, Farfel-Becker T, Sheng ZH. Revisiting LAMP1 as a marker for degradative autophagy-lysosomal organelles in the nervous system. *Autophagy*. 2018;14(8):1472-4.
46. Wilkinson RD, Williams R, Scott CJ, Burden RE. Cathepsin S: therapeutic, diagnostic, and prognostic potential. *Biol Chem*. 2015;396(8):867-82.
47. Wang Ip C, Kroner A, Fischer S, Berghoff M, Kobsar I, Maurer M, et al. Role of immune cells in animal models for inherited peripheral neuropathies. *Neuromolecular Med*. 2006;8(1-2):175-90.
48. Kokubun N. Charcot-Marie-Tooth disease and neuroinflammation. *Clinical and Experimental Neuroimmunology*. 2020;11(2):109-16.
49. Klein D, Groh J, Yuan X, Berve K, Stassart R, Fledrich R, et al. Early targeting of endoneurial macrophages alleviates the neuropathy and affects abnormal Schwann cell differentiation in a mouse model of Charcot-Marie-Tooth 1A. *Glia*. 2022;70(6):1100-16.
50. Liu WJ, Ye L, Huang WF, Guo LJ, Xu ZG, Wu HL, et al. p62 links the autophagy pathway and the ubiquitin-proteasome system upon ubiquitinated protein degradation. *Cell Mol Biol Lett*. 2016;21:29.
51. Cohen-Kaplan V, Livneh I, Avni N, Fabre B, Ziv T, Kwon YT, et al. p62- and ubiquitin-dependent stress-induced autophagy of the mammalian 26S proteasome. *Proc Natl Acad Sci U S A*. 2016;113(47):E7490-E9.
52. Horikoshi T, Arany I, Rajaraman S, Chen SH, Brysk H, Lei G, et al. Isoforms of cathepsin D and human epidermal differentiation. *Biochimie*. 1998;80(7):605-12.
53. Laurent-Matha V, Derocq D, Prébois C, Katunuma N, Liaudet-Coopman E. Processing of human cathepsin D is independent of its catalytic function and auto-activation: involvement of cathepsins L and B. *J Biochem*. 2006;139(3):363-71.
54. Hashimoto Y. Gelatin Zymography Using Leupeptin for the Detection of Various Cathepsin L Forms. *Methods Mol Biol*. 2017;1594:243-54.
55. Erdem S, Mendell JR, Sahenk Z. Fate of Schwann cells in CMT1A and HNPP: evidence for apoptosis. *J Neuropathol Exp Neurol*. 1998;57(6):635-42.
56. Sancho S, Young P, Suter U. Regulation of Schwann cell proliferation and apoptosis in PMP22-deficient mice and mouse models of Charcot-Marie-Tooth disease type 1A. *Brain*. 2001;124(Pt 11):2177-87.
57. Koike H, Iijima M, Mori K, Yamamoto M, Hattori N, Katsuno M, et al. Nonmyelinating Schwann cell involvement with well-preserved unmyelinated axons in Charcot-Marie-Tooth disease type 1A. *J Neuropathol Exp Neurol*. 2007;66(11):1027-36.

Acknowledgements – The authors are grateful to Research Foundation Flanders (FWO Vlaanderen) for granting this doctoral fellowship project to KL. ND would like to especially thank KL for the supervision during this senior internship and the entire FIERCE lab for their support and contributions.

Author contributions – KL, TV, and EW designed the research with the support of IL and LVDB. LVDB kindly provided the patient-derived iPSC and iPSC-SCP lines and the corresponding isogenic control cells. ND performed the experiments and data analysis under the supervision of KL, who also provided the mouse qPCR, primary mouse ICC data, and all WB samples, and with the guidance of HJ and JVDB. ND wrote the paper as part of her master's thesis, and KL edited the manuscript.

Supplementary information

Supplementary Table 1 – qPCR primer sequences.

Gene	Species	Primer pair sequence	
PMP22	Human	F 5' CTC TTC ACC AAG GG 3'	R 5' TGA CTT GAG TTT GAT TCA GCA AG 3'
LAMP-1	Mouse	F 5' AGG CCA CTG TGG GAA ACT CAT ACA 3'	R 5' TTC CAC AGA CCC AAA CCT GTC ACT 3'
	Human	F 5' CAG TTT GGC TCT GTG GAG GA 3'	R 5' GAG GTA GGC GAT GAG GAC GA 3'
CTD	Mouse	F 5' CTG CCC ACG GTC TAC CTG AA 3'	R 5' TTC CAC CCT GCG ATA CCT TG 3'
	Human	F 5' TAC ACG CTC AAG GTG TCG C 3'	R 5' GTG TAG TAG CGG CCG ATG AA 3'
CTB	Mouse	F 5' GGC TCT TGT TGG GCA TTT GG 3'	R 5' CTC GGC CAT TGG TGT GAA TG 3'
CTS	Mouse	F 5' CCC TAC AAA GCC ACG GAT GAA 3'	R 5' ACC AAA CGG GAG CTG AAT GT 3'
P62	Mouse	F 5' GGA CCC ATC TAC AGA GGC TG 3'	R 5' TCA TCC GAG AAA CCC ATG GAC 3'

Supplementary Table 2 – Primary antibodies for WB, ICC, and IHC.

Target	Species	Dilution	Company (reference)
LAMP-1	Rat	WB: 1/1000 ICC: 1/250 IHC: 1/200	Santa Cruz (sc-19992)
	Mouse	ICC: 1/250	DSHB (H413c)
CTD	Rabbit	WB: 1/1000 ICC: 1/250 IHC: 1/300	Abcam (ab75852)
CTB	Rabbit	WB: 1/1000 ICC: 1/250 IHC: 1/300	Abcam (ab214428)
p62	Mouse	ICC: 1/200	Abcam (ab56416)
UBIQ	Mouse	ICC: 1/150	Santa Cruz (sc-166553)
β-actin	Rabbit	WB: 1/1000	Novus (NB600-503SS)
	Mouse	WB: 1/1000	Santa Cruz (sc-47778)

List of abbreviations

AF = Alexa Fluor
Atg7 = autophagy-related 7
BME = β -mercaptoethanol
BSA = bovine serum albumin
CMT = Charcot-Marie-Tooth disease
CMT1/2/3/4 = Charcot-Marie-Tooth disease type 1/2/3/4
CMT1A = Charcot-Marie-Tooth disease type 1A
CMTX = X-linked Charcot-Marie-Tooth disease
CTB = cathepsin B
CTD = cathepsin D
CTS = cathepsin S
DMEM = Dulbecco's Modified Eagle Medium
DS-CTB = double chain CTB
DS-CTD = double chain CTD
ECAE = Ethical Committee for Animal Experimentation
ECM = extracellular matrix
F = forward primer
FACS = fluorescence-activated cell sorting
FBS = fetal bovine serum
FC = fold change
HMSN = hereditary motor and sensory neuropathy
ICC = immunocytochemistry
IHC = immunohistochemistry
iPSC = induced Pluripotent Stem Cells
iPSC-SCP = iPSC-derived Schwann cell precursors
ISO = isogenic control cells
LAMP-1 = lysosomal-associated membrane protein 1
LC3 = microtubule-associated protein light chain 3
LMP = lysosomal membrane permeabilization
LN₂ = liquid nitrogen
NCVs = nerve conduction velocities
NRG = neuregulin
P/S = penicillin/streptomycin
PBS = phosphate-buffered saline
PDGF-AA = platelet-derived growth factor AA
PFA = paraformaldehyde
PLL = poly-L-lysine
PMP22 = peripheral myelin protein 22
PVDF = polyvinylidene difluoride membrane
(q)PCR = (quantitative) polymerase chain reaction
R = reverse primer
RT = room temperature
SC = Schwann cells
SCP = Schwann cell precursors
SDS-PAGE = sodium dodecyl sulfate-polyacrylamide gel electrophoresis
SS-CTB = single chain CTB
SS-CTD = single chain CTD
UBIQ = ubiquitin
UPS = ubiquitin-proteasome system

WB = western blot

WT = wild type

w/o = week-old

YAC = yeast artificial chromosomal

y/o = year-old